Pakistan Veterinary Journal

ISSN: 0253-8318 (PRINT), 2074-7764 (ONLINE)
DOI: 10.29261/pakvetj/2026.198

RESEARCH ARTICLE

Coriolus versicolor Polysaccharide Mitigated Liver and Kidney Damage in Mice Exposed to Chromium

Jia Wang[1], Shiying Liao[2*], Bin Shi[3,4], Zhonghua Su[5], Mikhlid H. Almutairi[6], Zhen Yang[5*], Kun Li[1*]

[1]College of Veterinary Medicine, Nanjing Agricultural University, Nanjing 210095, PR China; [2]School of Basic Medicine, Hubei University of Arts and Science, Xiangyang 441053, China; [3]Institute of Animal Husbandry and Veterinary Medicine, Xizang Academy of Agricultural and Animal Husbandry Sciences, Lhasa 850009, China; [4]Key Laboratory of Animal Genetics and Breeding on Tibetan Plateau, Ministry of Agriculture and Rural Affairs, Lhasa 850009, China; [5]Animal Disease Prevention and Control Center of Xizang Autonomous Region, Lhasa Xizang 850000, China; [6]Department of Zoology, College of Science, King Saud University, P.O. Box 2455, Riyadh 11451, Saudi Arabia.
*Corresponding author: liaoshi71@163.com (SL); 1148893256@qq.com (ZY); lik2014@sina.com (KL)

ARTICLE HISTORY (26-896)

Received: July 23, 2026
Revised: August 24, 2026
Accepted: August 26, 2026
Published online: August 30, 2026

Key words:
Coriolus versicolor
Polysaccharide
Cr (VI)
Metabonomics
Mice
Microbiota

ABSTRACT

Heavy metal pollution not only causes great harm to the environment but also threatens the health of animals and humans. The current study investigated the effect of Tibetan *Coriolus versicolor* polysaccharide on mice exposed to Chromium (Cr). Thirty mice (BALB/C) were used in experiments and divided into the following groups, *i.e.*, CCR (control), CMR (Cr model group), and CYR (treatment group). Mice in the CMR and CYR groups were given Potassium dichromate (10mg/kg) daily by gavage for about thirty-five days, and WR mice were treated with CVP (25mg/kg) via gavage. Pathological analysis indicated that CVP could effectively decrease tissue damage and fibrosis in mice. Organ index analysis found that CVP increased indexes of the heart ($P<0.05$) and kidney ($P<0.0001$), while reducing indexes of the liver ($P<0.0001$) and spleen ($P<0.05$) in mice. Serum biochemical analysis showed that CVP significantly decreased the contents of AST ($P<0.0001$), ALT ($P<0.0001$), BUN ($P<0.001$), and Creatinine ($P<0.0001$) in mice. CVP up-regulated the expression levels of NQO-1 ($P<0.01$), Nrf-2 ($P<0.01$), and IL-10 ($P<0.05$), and decreased IL-6 ($P<0.0001$), TNF-α ($P<0.01$), and Bax ($P<0.001$) expression. Microbiome analysis found five phyla (Firmicutes A, Firmicutes B, Desulfobacterota I, Firmicutes C, Deferribacterota) and twenty-one genera were different among groups. Those genera were *Mailhella*, *Lawsonibacter*, *Anaerotruncus*, *Angelakisella*, *Merdisoma*, *Allobaculum,* etc. The number of metabolites identified in mice was 3391, with 35 in CCR, CMR, 189 in CMR, CRY, and 180 in CCR and CYR, respectively. We demonstrated that Tibetan *Coriolus versicolor* polysaccharide could effectively alleviate liver and kidney damage in mice exposed to chromium by regulating antioxidant ability, inflammatory response, apoptosis, and intestinal microbiota in mice.

To Cite This Article: Wang J, Liao S, Shi B, Su Z, Almutairi MH, Yang Z, Li K, 2026. *Coriolus versicolor* polysaccharide mitigated liver and kidney damage in mice exposed to chromium. Pak Vet J, 46(8): 1920-1933. http://dx.doi.org/10.29261/pakvetj/2026.198

INTRODUCTION

Heavy metal pollution not only causes great harm to the environment but also threatens the health of animals and humans (Yin *et al*., 2019; Aljohani, 2025). Due to rapidly increasing urbanization and industrialization, environmental pollution, especially that of heavy metals, is an emerging and deadly threat to public health, with millions of young children dying annually due to the toxic effects of heavy metals (Pushkar *et al*., 2021; Saleem *et al*., 2025). Among heavy metals, Chromium is a unique heavy metal, while the stable forms include trivalent and hexavalent forms that exist in nature (Alvarez *et al*., 2021). In industry, widely used metal for metallurgy, electroplating, chrome plating, and paint, and is present in large quantities in industrial waste (He and Li, 2020). This element presents different chemical properties in its different oxidation states. Cr (III) is an important and essential nutrient, which is widely used as a food supplement, as it can block the adverse impact of glycolipid metabolism and is beneficial to growth (Li *et al*., 2022). Cr (VI) is a strong oxidant with severe toxicity, which is listed as a class I carcinogen to humans (Kazakis *et al*.,

2017). Previously, studies found that Cr (VI) could lead to bleeding, liver and kidney damage, respiratory illness, and cancer in people (Hedberg, 2020; Tumolo *et al*., 2020). Therefore, finding novel products to mitigate damage caused by heavy metals has become urgent and necessary (Zhao *et al*., 2022).

Coriolus versicolor is a well-known traditional medical mushroom in China, which is also known as Yunzhi in China and Turkey Tail in Western countries (Habtemariam, 2020). This fungus has the value of promoting health and longevity (Wang *et al*., 2015). Previous studies reported that the polysaccharides from *Coriolus versicolor* have bio-functions of immune adjustment, anti-tumor, anti-inflammation, and anti-virus (Gariboldi *et al*., 2023), which were also used in cancer therapy (Zhong *et al*., 2019). The structural data of Tibetan *Coriolus versicolor* polysaccharide is a complex compound composed of different simple sugars such as glucose, galactose, mannose, and fucose, with minor amounts of other monosaccharides. The polysaccharide consists of more than one monosaccharide linked with each other through β-(1→3) linkages known as glucopyranosyl units, with branching at the O-6 position and side chains containing β-(1→6)-linked galactose or mannose residues. The molecular weight distribution typically falls within the range of 20–100kDa, depending on extraction and purification methods. The triple-helical conformation observed in aqueous solution is believed to be crucial for its bioactivity, including immunomodulatory, antioxidant, and antitumor effects (Rau *et al*., 2009).

Intestinal microflora consists of billions of microbes, for instance, bacteria, archaea, protozoa, *etc*. (Liang *et al*., 2025; Xu *et al*., 2025), which positively contributes to the balance of the intestinal environment, metabolism, immune activity, and neural function (Che *et al*., 2022). Recent studies revealed that imbalance in intestinal microbiota results liver damage, cardiovascular disease, and inflammatory bowel disease (Chen and Wang, 2022; Rahman *et al*., 2022; Hsu and Schnabl, 2023), while polysaccharides could alleviate the intestine micro-balance (Fang *et al*., 2022; Chen *et al*., 2023) However, very limited knowledge is available about the effect of *Coriolus versicolor* polysaccharide on mice exposed to chromium. Hence, the current research was performed to investigate the alleviating effects of Tibetan CVP on liver and kidney injuries in mice exposed to chromium through multi-omics studies.

MATERIALS AND METHODS

Coriolus versicolor polysaccharide extraction: *Coriolus versicolor* (300gm) was purchased from a local pharmaceutical company, Lhasa, Tibet. Then the CVP was extracted as previously described (Bi *et al*., 2024). In brief, CM powder was dissolved in 95% ethanol solution (1:20 w/v) and ultrasound-treated for half an hour. Then, it was recovered twice with sterile water at 1:10w/v at 100ºC. After that, the crude polysaccharides were obtained by deproteinizing with a sevage reagent (Ying *et al*., 2020). Finally, the crude polysaccharides were dialyzed via a dialysis bag (3500 Da) and freeze-dried into powder for further use. The concentration of CVP was measured via the phenol-sulfuric acid method (Song *et al*., 2023).

Experimental design for trial on animals: All the experimental procedures were approved and explained by the Nanjing Agricultural University animal ethics committee, and animals were fed in the NAU animal laboratory center. A total of thirty-four 238-day-old BALB/C laboratory mice (23.18±1.26gm) were purchased from the Animal Breeding and Production Center of Qinglongshan Animal Breeding (Nanjing, China). Subsequently, three days of accommodation, the animals were divided into CCR (control), CMR (Cr model group), and CYR (treatment group), with ten mice in each group. Mice in groups CMR and CYR were given Potassium dichromate ($K_2Cr_2O_7$, 10mg/kg) daily via gavage, and mice in WR were treated with CVP (25mg/kg) via gavage, while animals in groups CR and MR were induced with an equivalent amount of sterile water. All mice were fed in a standardized environment, and on the 36th day, all animals were euthanized by employing CO_2 inhalation to collect blood, organ, and intestine samples. The body weight and organ weight were documented.

Serological examination: For serological analysis, serum was extracted from all blood samples separately through centrifugation at 3500xg for about 20min. Different biomarkers used for liver and kidney function (AST, ALT, creatinine, BUN), antioxidant ability (T-AOC, GSH-Px, SOD, MDA), and inflammatory factors (IL-6, IL-10, IL-1β, TNF-alpha) were measured through commercial ELISA kits according to a previous study (Goraya *et al*., 2025; Chen *et al*., 2026).

Analysis of vital organs for histopathological changes: Samples of different vital organ tissues such as liver, spleen, and kidney from treatment groups CCR, CMR, and CYR were collected and preserved in 4% paraformaldehyde solution and sent for H&E and Sirius red staining to Pinuofei Biological Technology (Wuhan, China). Histopathological analysis was performed using a microscope (CX43) from Olympus Co. (Japan).

RT-qPCR analysis: Tissues (200mg/mouse) of liver from mice in all groups were homogenized to extract RNA using Trizol reagent (Invitrogen, USA). Then, these RNA products were converted into cDNA using a cDNA synthesis kit (Yeasen, China). RT-qPCR was then performed by employing TaqMan multiplex qPCR master mix (Yeasen, China), and relative mRNA expression levels among mice in different groups were analyzed via the $2^{-\triangle\triangle Ct}$ method (Table 1).

Table 1: Primer sequences used for qRT-PCR

Gene	Forward sequences (5′—3′)	Reverse sequences (5′—3′)
TNF-α	GTGGAACTGGCAGAAGAG	GAGAAGAGGCTGAGACATAG
NQO 1	ATGAAGGAGGCTGCTGTA	AGATGACTCGGAAGGATACT
HO-1	GCCTTCCTGCTCAACATT	AAGTGACGCCATCTGTGA
IL-6	TCCATCCAGTTGCCTTCT	TAAGCCTCCGACTTGTGA
IL-10	GGTTGCCAAGCCTTATCG	TCTTCACCTGCTCCACTG
Nrf2	CTACAGTCCCAGCAGAGT	CTCAGAAACCTCCTTCCAAA
Bcl2	GAGATCGTGATGAAGTACA TAC	CAGGCTGGAAGGAGAAGA
Bax	GATGCGTCCACCAAGAAG	CCAGTTGAAGTTGCCATCA
GAPDH	TCTCCTGCGACTTCAACA	TGTAGCCGTATTCATTGTCA

Western blotting assay: The liver tissue proteins of mice in all groups were collected in RIPA buffer with PMSF and inhibitors, and the liver sample extract concentration was measured using a BCA assay kit (Vazyme, China). (Vazyme, China). Western blotting loading buffers were mixed with protein products and denatured in 100ºC boiling water for 5

min, and then they were separated by SDS-polyacrylamide gel electrophoresis (10%). After that, proteins were transferred to polyvinylidene fluoride, blocked with skimmed milk (5%), and incubated with the primary antibodies from Abclonal, China. Finally, those PVDF membranes were washed, incubated with the secondary antibodies, and examined using an enhanced chemiluminescence reagent (Vazyme, China) as depicted in a recent study (Wang *et al*., 2023). The antibodies used in this study were Bax (A20227, 21kDa) and β-Actin (AC026, 42kDa).

Microbiome sequencing and bioinformatics analysis: Total DNA from the rectums of mice in CCR, CMR, and CYR groups (n=6) was extracted using a genomic extraction kit (Tiangen, China). Then, all the products of regions V3-V4 were amplified using 16S rRNA targeting primers (338F/ 806R) (Tu *et al*., 2022), and those amplified genes were also examined by NanoDrop NC2000 and agarose gel electrophoresis. After that, the Fast-Pure gel DNA extraction mini kit (Vazyme, China) and Quant-iT PicoGreen dsDNA assay kit (Invitrogen, USA) were used for purification and quantification of 16S rRNA amplified bands, respectively. Finally, Illumina (MiSeq) platform from Wuhan Bioyi Biotechnology Co., Ltd (China) was performed to get paired-end sequencing (2×300bp).

Later, the bioinformatics analysis was carried out using QIIME2 with slight modifications (https://docs.qiime2.org/2023.7/tutorials/) (Balzerani *et al*., 2024). First, the current raw sequences were demultiplexed, quality-filtered, and merged via the DADA2 plugin (Kim *et al*., 2021). Second, non-singleton amplicon sequence variants (ASVs) were generated by aligning sequences with MAFFT, and a phylogeny was constructed through fasttree2 (Price *et al*., 2010; Katoh and Standley, 2013). Third, alpha-diversity metrics were calculated via QIIME2. Also, beta diversity was analyzed using PCA, PCoA, NMDS, and UPGMA (Tarrah *et al*., 2022). Fourth, the shared and unique ASVs among different groups were visualized in R using a Venn diagram (Li *et al*., 2024; Liu *et al*., 2024). LEfSe and t-tests were used to reveal the marked different taxa across groups using the default module (Peng *et al*., 2024). Fifth, the function of the intestinal microbiome of all mice was predicted by PICRUSt2 targeting MetaCyc and databases (Douglas *et al*., 2020).

Metabolomics analysis: Eighteen liver samples from CCR, CMR, and CYR groups were used to extract metabolites for LC-MS/MS detection, as reported in previous work (Want *et al*., 2013). The UHPLC-MS/MS in positive/negative polarity mode was performed via the Vanquish UHPLC system and Orbitrap Exploris 120 mass spectrometer from Thermpo-Fisher (Germany) at Wuhan Bioyi Biotechnology Co., Ltd., China.

All the raw data were processed via Compound Discoverer (3.3) to perform metabolite quantification analysis (Cooper and Yang, 2024). The annotation of current metabolites was performed by employing databases of KEGG, HMDB, and LIPIDMaps. After that, PLS-DA and PCA were employed using metaX (Wen *et al*., 2017). Differences among mice in different groups was explored via One-way ANOVA, and when the P-vale of metabolites with P-values less than 0.05 and VIP greater than 1 were identified as differential metabolites in the groups (Wang *et al*., 2023). The clustering heat map and Volcano plots were created using ggplot-2. The role of these metabolites and related pathways was examined through the KEGG database (Zhang *et al*., 2023).

Correlation analysis: The analysis of Spearman correlation was performed to evaluate the relationship between the physiological index and the abundance of bacteria and metabolites in the mouse gut, as already studied in previous research (Wang *et al*., 2020).

Statistical analysis: All the current data were examined through One-way-ANOVA and Dunnett's test (SPSS, 26.0). Results were displayed as means ± SD, and significance was recognized when $P<0.05$.

Table 2: The sequenced data information of mice in different groups

Samples	Input	Filtered	Denoised	Merged	Non-chimeric
CCR1	63806	59411	58929	57259	49672
CCR2	57991	53479	51515	39590	30741
CCR3	78420	72994	72786	71646	54579
CCR4	69570	64901	63708	55938	44594
CCR5	73050	67711	65771	52987	37994
CCR6	73830	67860	66628	57260	44042
CMR1	78580	72831	70182	57148	40273
CMR2	77913	71957	68884	53660	39670
CMR3	81792	75382	72166	55544	42540
CMR4	73056	67544	63977	44067	32955
CMR5	80869	75235	72486	56893	37055
CMR6	77961	71692	68079	47021	34690
CYR1	83371	76981	75283	65323	52222
CYR2	71773	66336	64586	54394	36900
CYR3	70193	64603	62791	53625	39686
CYR4	49453	45592	44728	40394	31447
CYR5	68203	63237	61801	56237	36932
CYR6	66287	61161	58409	44403	33697

Table 3: Alpha diversity analysis of mice in different groups

Sample	Chao1	Faith_pd	Goods_coverage	Observed_species	Pielou_e	Shannon	Simpson
CCR1	178.6701277	29.13733155	0.998968884	166.9	0.406376452	3.000111788	0.704167477
CCR2	3339.353934	186.5197066	0.985908077	3259.9	0.753212064	8.790444495	0.957969003
CCR3	92.28338328	14.86870341	0.999513693	83.7	0.527789847	3.370817875	0.768616847
CCR4	2466.286741	119.2230647	0.978609821	2184.4	0.590860703	6.554426854	0.847616559
CCR5	3167.838396	185.7083746	0.976426926	2929.5	0.710171375	8.17864328	0.971176317
CCR6	2115.712981	124.4529468	0.981480127	1858.3	0.589248621	6.399096005	0.907217127
CMR1	2004.660098	175.580103	0.98606896	1854.2	0.704303913	7.64631919	0.973203835
CMR2	3436.100309	207.6830763	0.975457969	3194.3	0.720893929	8.39212883	0.964048946
CMR3	2560.396921	184.7406811	0.9813229	2340.5	0.695884891	7.788753891	0.944213394
CMR4	2938.26628	201.9838386	0.986705181	2848.8	0.80131815	9.196037377	0.987121356
CMR5	2532.569889	174.5870503	0.985355955	2410	0.745073948	8.370765486	0.984302646
CMR6	3319.098648	203.2805199	0.982595342	3198.5	0.798877674	9.301472597	0.98608109
CYR1	2338.35327	141.7934443	0.977607956	1991.9	0.478639689	5.245848566	0.728515881
CYR2	2538.24881	152.7766826	0.984145673	2392.2	0.746310784	8.376680356	0.97968786
CYR3	1861.637402	132.8083727	0.987725328	1736.7	0.634070882	6.823932674	0.932904644
CYR4	825.2154898	68.86560614	0.997733007	811.5	0.625660975	6.046661263	0.926745826
CYR5	1230.465466	96.52329094	0.99432886	1184.8	0.669017385	6.830941593	0.961868623
CYR6	2695.36995	175.1284695	0.986961132	2602.5	0.759262227	8.614342439	0.978020921

RESULTS

CVP prevented organ damage in mice induced by Cr (VI): The weekly body weight of mice in group CMR was lower than CCR, while mice treated with CVP increased weight in CYR (Fig. 1a). Cr (VI) decreased the net weight rate in mice in CMR ($P<0.05$), while CVP could promote the growth of mice in CYR (Fig. 1b). Organ index analysis found that Cr (VI) significantly decreased the index of the heart ($P<0.01$) and kidney ($P<0.0001$), while increasing the indexes of the liver ($P<0.001$) and spleen ($P<0.05$) in mice in CMR. Interestingly, CVP increased indexes of index of heart ($P<0.05$) and kidney ($P<0.0001$), while decreased indexes of liver ($P<0.0001$) and spleen ($P<0.05$) in mice (Fig. 1c). Serum biochemical analysis disclosed that the contents of AST ($P<0.0001$), ALT ($P<0.0001$), Bun ($P<0.001$) and creatinine ($P<0.0001$) were observably higher in Cr (VI) induced mice, while CVP markedly decreased them in animals (Fig. 1d-e). Histopathology indicated that Cr (VI) caused cellular degeneration, infiltration of inflammatory cells, and hemorrhages in the liver and kidney, while CVP could effectively decrease tissue damage in mice (Fig. 2a). Sirius red staining showed that Cr (VI) caused tissue fibrosis in mice in group CMR, while CVP significantly reduced the degree in animals (Fig. 2b).

CVP regulated inflammation levels and oxidation resistance in mice induced by Cr (VI): The contents of T-AOC ($P<0.05$), GSH-Px ($P<0.01$), SOD ($P<0.05$) and IL-10 ($P<0.05$) were lower in mice induced by Cr (VI), while MDA ($P<0.0001$), IL-6 ($P<0.01$), IL-1β ($P<0.001$) and TNF-α ($P<0.01$) were signally higher. Surprisingly, T-AOC ($P<0.001$), GSH-Px ($P<0.001$), SOD ($P<0.01$) and IL-10 ($P<0.01$) were memorably increased by the treatment of CVP and MDA ($P<0.01$), IL-6 ($P<0.05$), IL-1β ($P<0.05$) and TNF-α ($P<0.001$) were also decreased in treated mice (Fig. 3a). Relative gene expression analysis showed that Cr (VI) inhibited the expressions of NQO-1 ($P<0.001$), Nrf-2 ($P<0.01$) and IL-10 ($P<0.001$), while promoting the expressions of IL-6 ($P<0.0001$), TNF-α ($P<0.001$) and Bax ($P<0.001$). However, animals treated with CVP had higher expression levels of NQO-1 ($P<0.01$), Nrf-2 ($P<0.01$) and IL-10 ($P<0.5$) and liver levels of IL-6 ($P<0.0001$), TNF-α ($P<0.01$) and Bax ($P<0.001$) (Fig. 3b). Protein analysis showed that mice induced by Cr (VI) significantly expressed Bax than mice in group CCR ($P<0.0001$) and CYR ($P<0.0001$) (Fig. 3c).

CVP restored gut microbiome composition and function of mice induced by Cr (VI): The sequence information of mice was shown in Table 2, and those sequences were aligned to 9356 (CCR), 14277 (CMR), and 9531 (CYR) ASVs in mice in different groups, with 656 common ASVs (Fig. 4a). The rarefaction curves and rank abundance curves in the current mice were straight and horizontal, which showed higher diversity and evenness of obtained samples (Fig. 4b-c). Alpha diversity analysis found that Faith-PD was markedly higher in CRM ($P<0.05$), although no distinct difference in other indices among different groups was detected (Table 3, Fig. 4d).

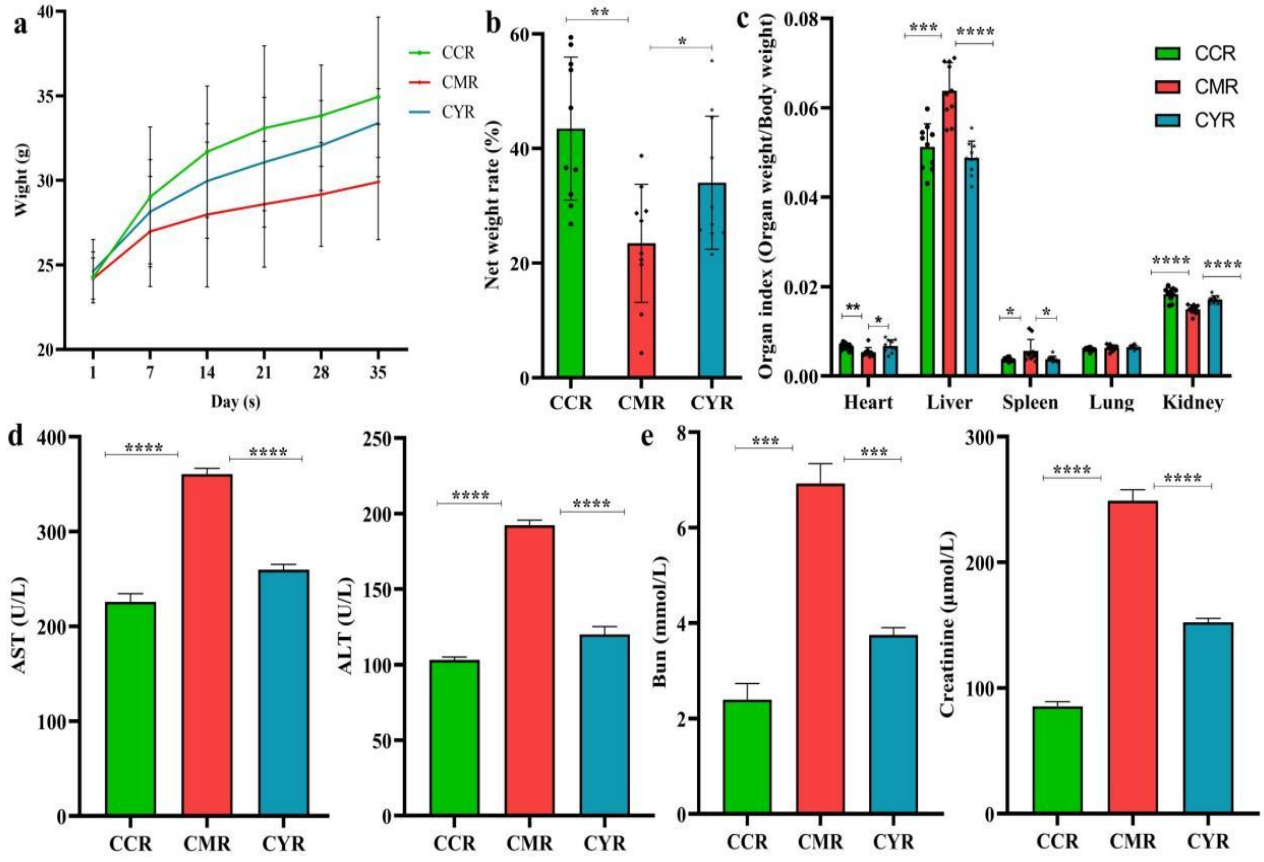

Fig. 1: CVP helps the body status of mice given by Cr (VI). a: body weight, b: net weight rate, c: organ indices, d: liver function, e: kidney function. Data were presented as the mean ± SME. *P<0.05; **P<0.01; ***P<0.001 and ****P<0.0001.

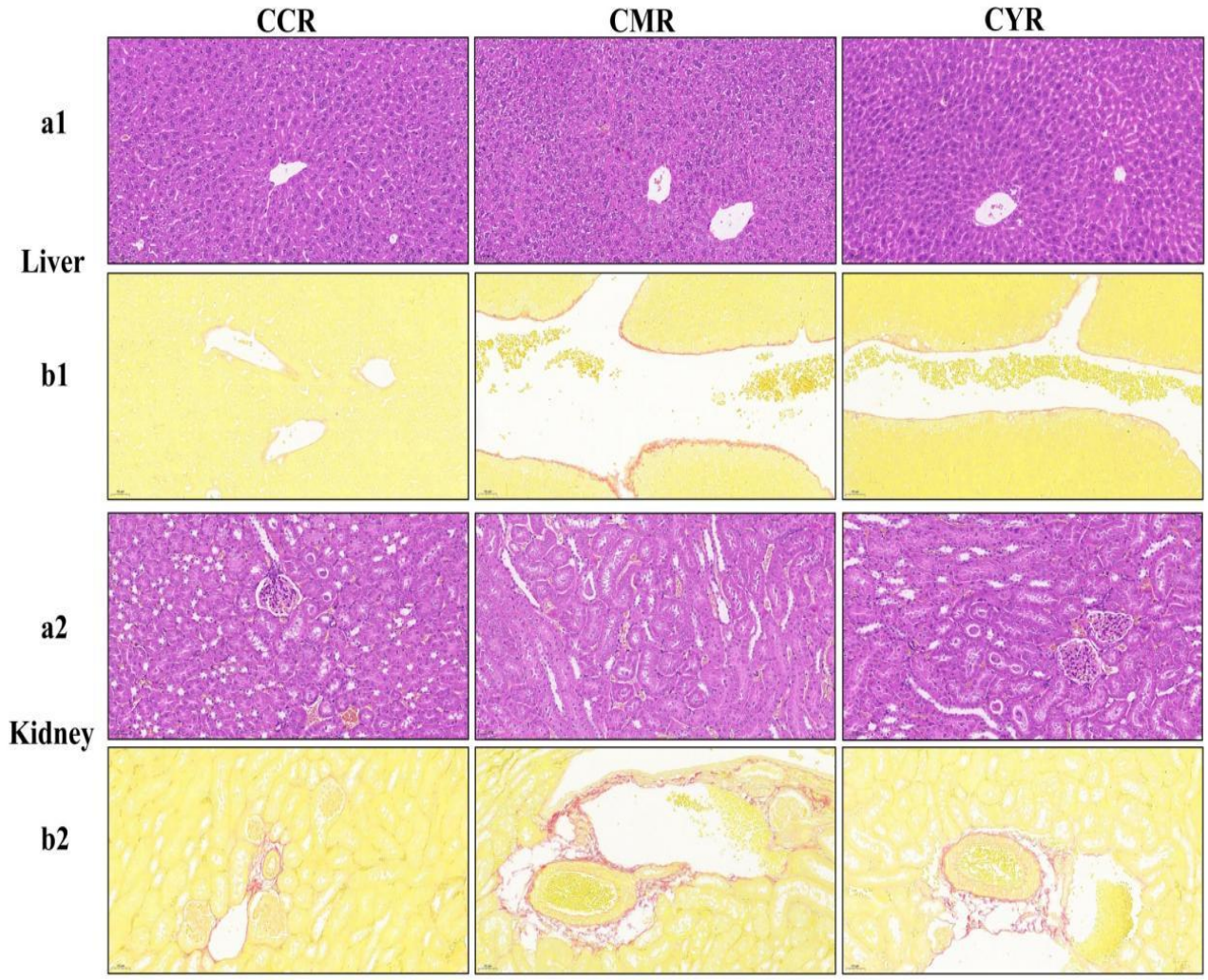

Fig. 2: CVP mitigates organ damage in mice induced by Cr (VI). a: H&E staining (a1: liver, a2: kindly), b: Sirus red staining (b1: liver, b2: kindly).

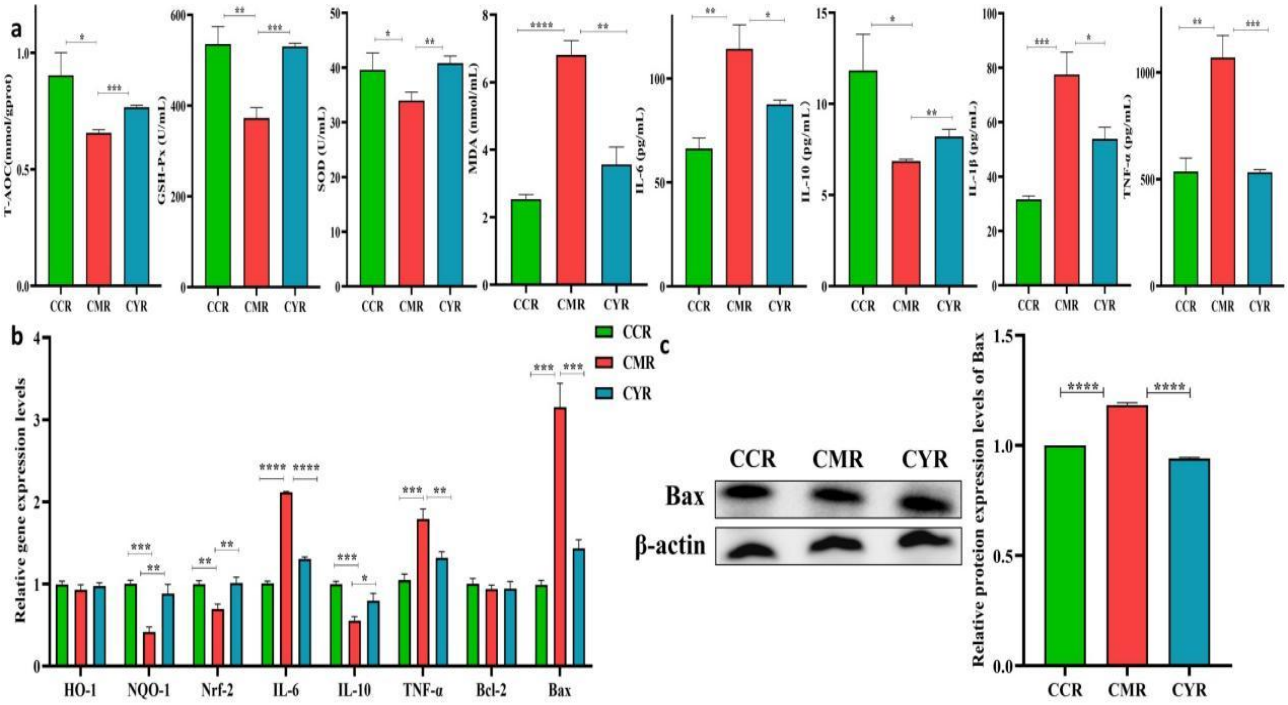

Fig. 3: CVP-regulated inflammatory response and oxidative stress in mice induced by Cr (VI). a: levels of inflammatory factors and contents of antioxidases, b: Relative gene expressions, c: Relative protein expressions. Significance is presented as *P<0.05; **P<0.01; ***P<0.001 and ****P<0.0001; data were presented as the mean ± SEM.

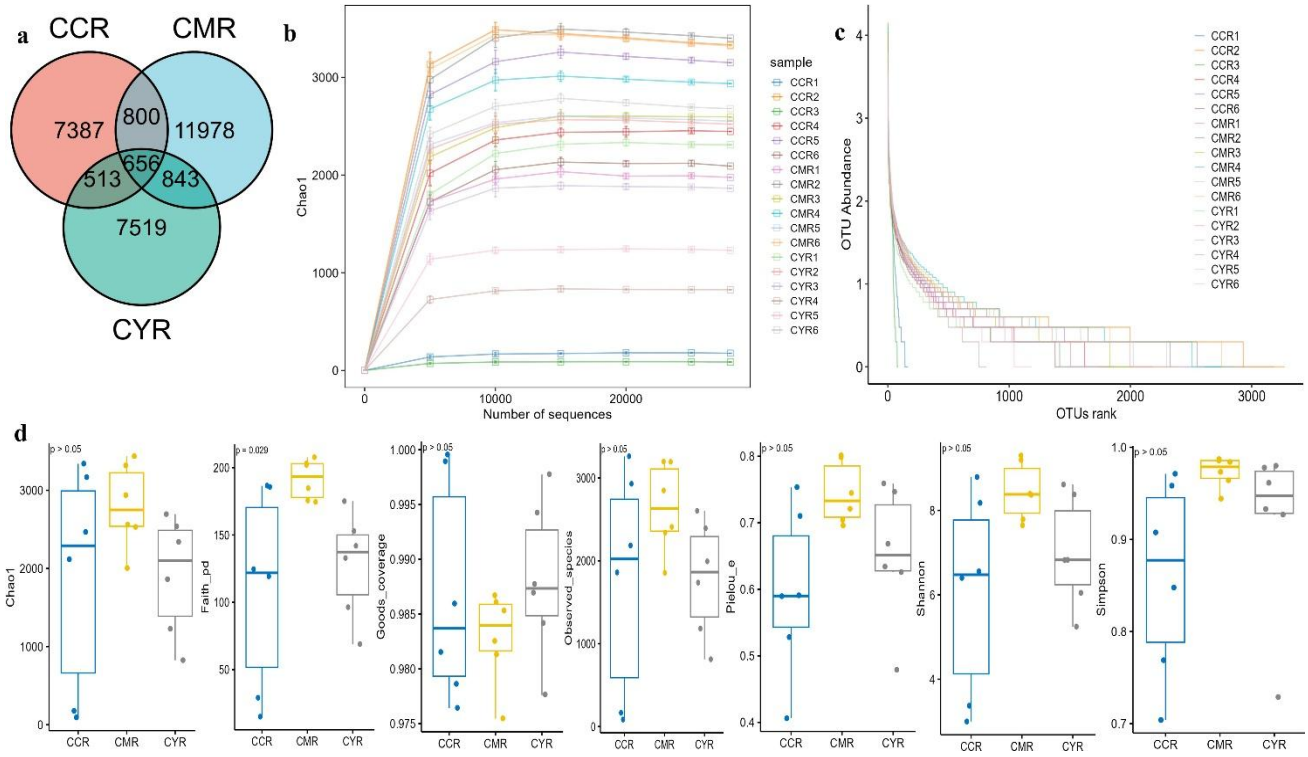

Fig. 4: Venn map and alpha diversity analysis of mice in different groups. a: Venn diagram, b: Rarefaction curve, c: Rank abundance curve, d: alpha diversity indices.

The main phyla at phylum level, in different groups were Firmicutes_D (34.26%), Bacteroidota (31.00%) and Campylobacterota (19.85%) in CCR, Bacteroidota (44.00%), Firmicutes_A (17.96%), Desulfobacterota_I (12.28%) in CMR, Bacteroidota (37.99%), Firmicutes_D (33.42%) and Verrucomicrobiota (9.48%) in CYR (Fig. 5a). At the class level, the prime classes in group CCR were Bacilli (34.26%), Bacteroidia (40.00%) and Campylobacteria (19.85%), in group CMR were Bacteroidia (44.00%), Clostridia_258483 (17.96%), Desulfovibrionia (12.28%), and in group CYR were Bacteroides (37.99%), Bacilli (33.43%) and Verrucomicrobiae (9.48%), respectively (Fig. 5b). At the order level, the dominating classes in different groups were Lactobacillales (32.47%), Bacteroidales (30.73%), and Campylobacterales (19.86%) in CCR, Bacteroidales (42.67%), Desulfovibrionales (12.43%), Lactobacillales (10.91%) in CMR, Bacteroidales (36.96%), Lactobacillales (32.94%) and Verrucomicrobiales (9.55%) in CYR (Fig. 5c). At the family level, the staple families in different groups were Lactobacillaceae (31.93%), Muribaculaceae (24.64%) and Helicobacteraceae (19.89%) in CCR, Muribaculaceae (30.23%), Desulfovibrionaceae (12.61%) and Lachnospiraceae (10.91%) in CMR, Lactobacillaceae (33.03%), Muribaculaceae (26.51%) and Akkermansiaceae (9.90%) in CYR (Fig. 5d). At the genus level, the considerable genera in different groups were *Lactobacillus* (19.65%), *Ligilactobacillus* (13.57%), *Mucispirillum* (10.63%) in CCR, Mailhella (13.32%), *Paramuribaculum* (9.10%), *Lactobacillus* (7.72%) in CMR, *Lactobacillus* (25.54%), *Akkermansia* (11.55%) and *Paramuribaculum* (10.14%) in CYR (Fig. 5e).

Beta diversity indicated that the relative distance between group CCR and CYR was closer than between group CCR and CMR, as revealed by PCoA (Fig. 6a1), NMDS (Fig. 6a2) and UPGMA (Fig. 6a3). The group difference was also confirmed by PERMANOVA analysis ($P<0.05$). The heat map showed that phyla of Firmicutes C, Firmicutes G, Campylobacterota, and Deferribacterota were higher in CCR, Proteobacteria, Firmicutes B370539, Deinococcota, Patescibacterota, Planctomycetota, Cyanobacteria, Firmicutes A and Actinobacteriota were higher in CRM, while Verruomicrobiota, Nitrospirota A 437815, Eisenbacteria, Gemmatimonadota, Methylomirabilota, Myxococcota A 473307 and Acidobacteriota (Fig. 6b1). Genera of *Rikenelia*, UBA7173, *Mammaliicoccus* 3179276, *Corynebacterium*, UBA3282, *Psychrobacter*, *Facklamia* A 32262, *Aerococcus*, *Clostridium* T, *Enterenecus*, *Staphylococcus*, COE1, CAG-485, *Desulfovibrio* R 446353, *Kineothrix,* and *Lawsonibacter* were higher in CMR, *Helicobacter* D, *Mucispirillum*, *Helicobacter* C 479931, *Ligilactobacillus*, *Ruminococcus* C 58660 and *Malacoplasma* A 271108 were higher in CCR, while *Eubacterium* R was higher in CYR (Fig. 6b2).

LEfSe analysis showed 37 significantly different bacteria among the three mouse groups, and the top ten species in each group were shown in the cladogram (Fig. 6). Among them, Mycoplasmatales ($P<0.05$), Malacoplasma A 271108 ($P<0.05$), and Mycoplasmoidaceae ($P<0.05$) were signally higher in CCR, Desulfovibrionaceae ($P<0.01$), Desulfovibrionales ($P<0.05$), Desulfovibrionia ($P<0.05$), Desulfobacterota I ($P<0.01$), Mailhella ($P<0.01$), Clostridia 258483 ($P<0.05$), Firmicutes A ($P<0.05$), Lachnospirales ($P<0.01$), Lachnospiraceae ($P<0.01$) and Kineothrix ($P<0.01$) were observably higher in CMR, while Peptostreptococcaceae 256921 ($P<0.05$) and Peptostreptococcales ($P<0.05$) were obviously higher in CYR group (Fig. 7).

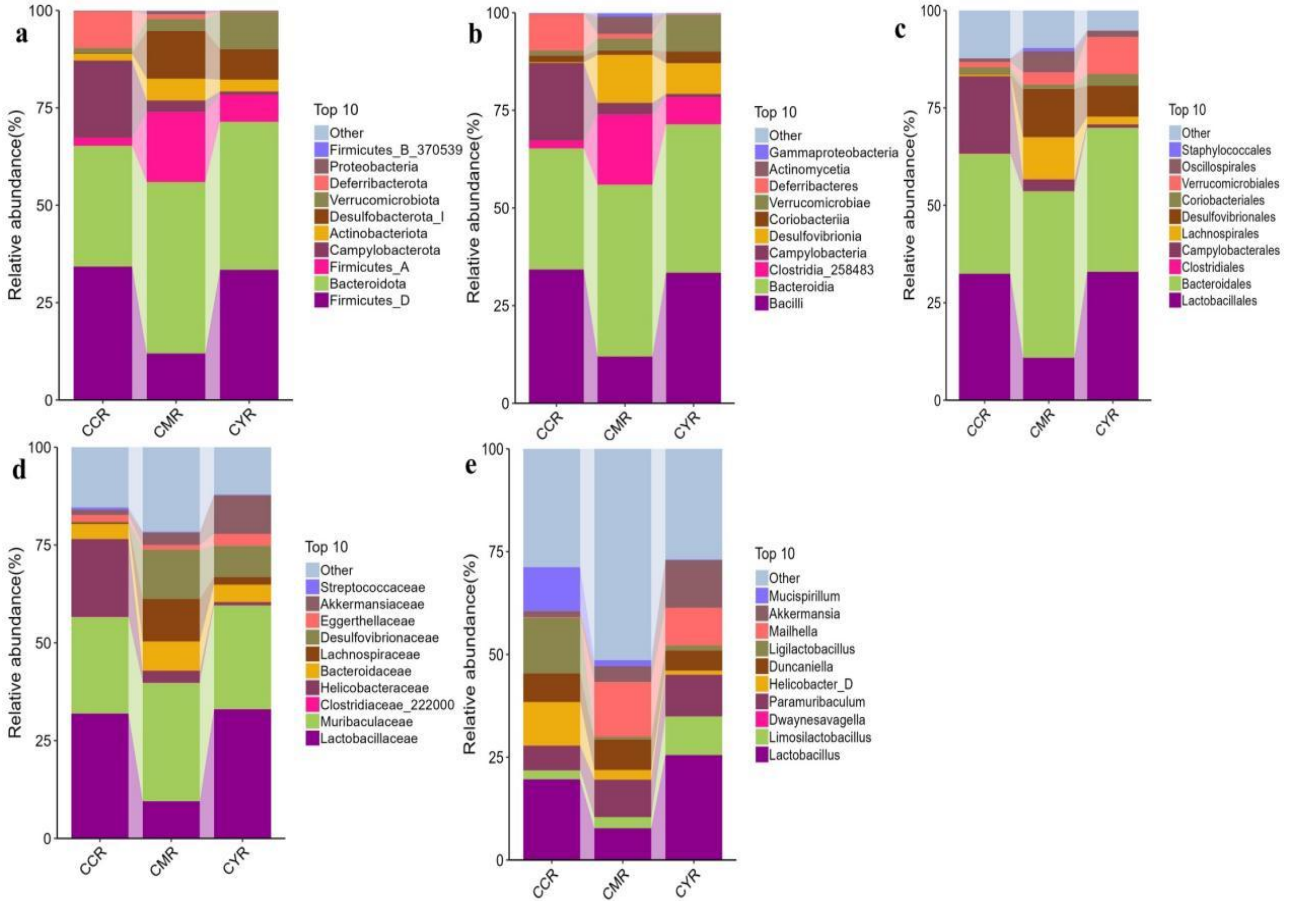

Fig. 5: Analysis of microbiota composition of mice induced by Cr (VI) in different taxa, i.e., a: Phylum, b: Class, c: Order, d: Family, and e: Genus.

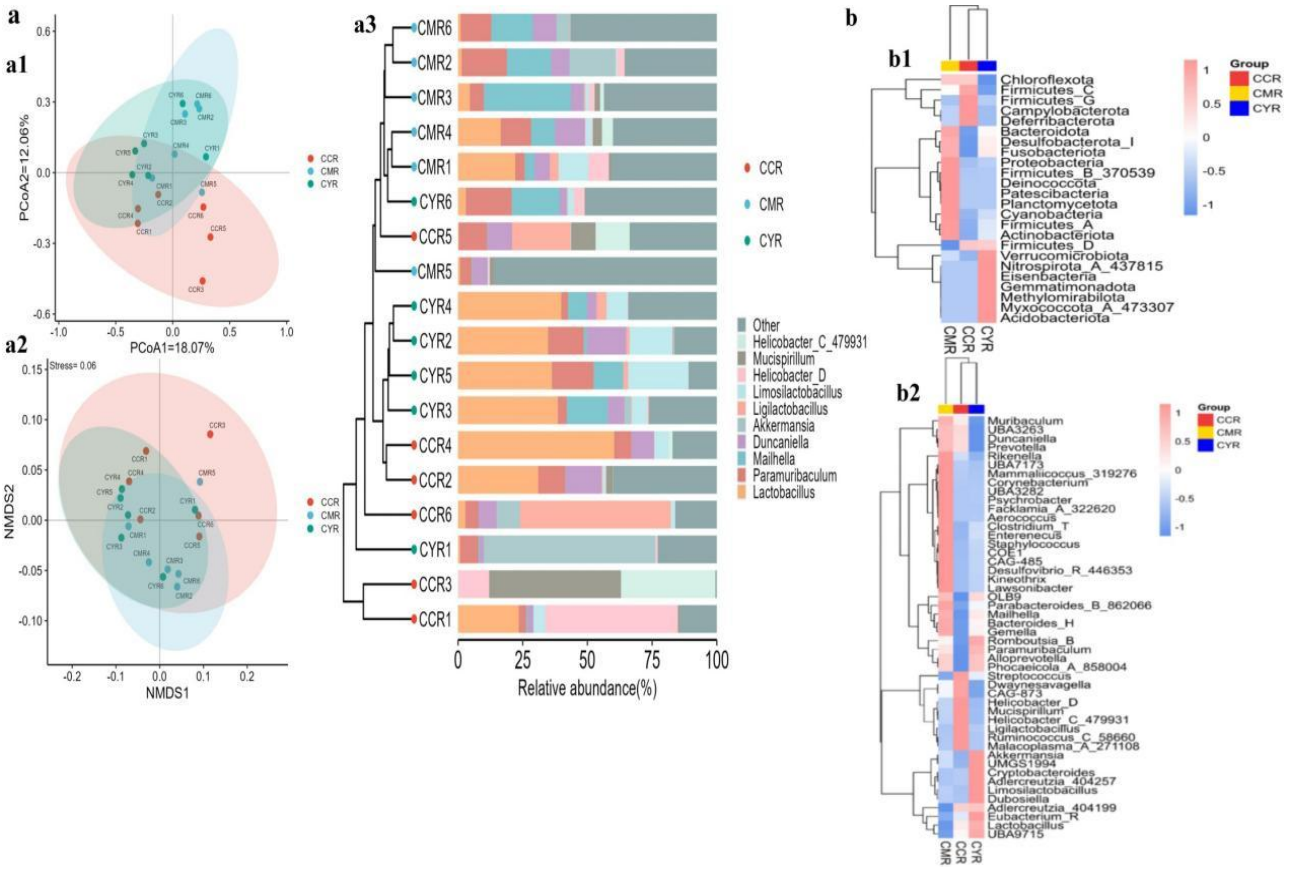

Fig. 6: Analysis of β-diversity and heat map of intestinal microbiota of mice induced by Cr (VI). a: Beta diversity (a1: PCoA, a2: NMDS, a3: UPGMA clustering analysis), b: Heat map (b1: Phylum, b2: Genus).

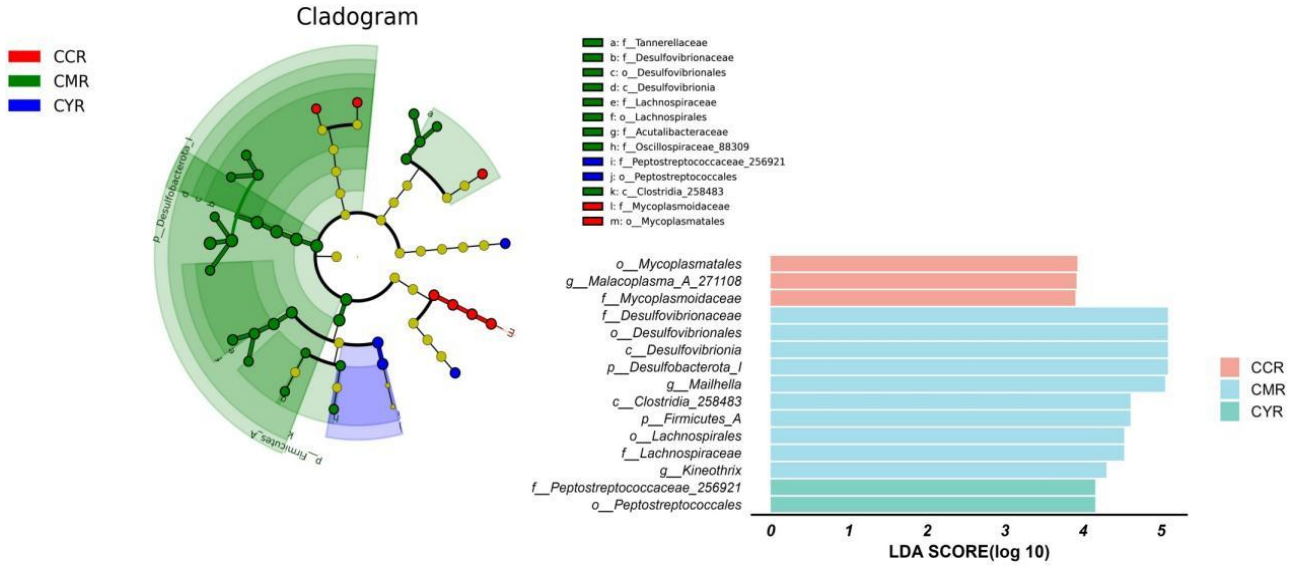

Fig. 7: Marker species of mice in various groups studied by LEfSe.

Analyzing via T-test showed that phyla of Firmicutes A (P<0.01) and Firmicutes B 370539 (P<0.05) were meaningfully higher in CMR than CCR and CYR, Desulfobacterota I was lower in CCR than CMR (P<0.05) and CYR (P<0.05), Firmicutes C was signally lower in CYR than CCR (P<0.01) and CMR (P<0.05), and Deferribacterota was observably higher in CMR than CYR (P<0.05) (Fig. 8a). Genera of *Mailhella* in CCR was lower than CMR (P<0.05) and CYR (P<0.05). *Lawsonibacter* (P<0.05), *Anaerotruncus* (P<0.05), *Angelakisella* (P<0.05), *Merdisoma* (P<0.05), and *Allobaculum* (P<0.05) were expressively higher in CMR than in CCR and CYR. *Mucispirillum* (P<0.05), *Prevotella* (P<0.05), *Tidjanibacter* (P<0.05), and *Choladousia* (P<0.05) were expressively higher levels in CMR than in CYR. OLB9 (P<0.05), *Enterobacter* (P<0.05), *Odoribacter* 865974 (P<0.05), CAG-95 (P<0.05), *Acetobacter* (P<0.05), and *Cupidesulfovibrio* (P<0.05) were observably higher in CMR than in CCR. *Gemella* (P<0.05) and CAG-83 (P<0.05) were significantly higher in CYR than in CCR, whereas *Veillonella* A (P<0.05) was meaningfully lower in CYR. *Adlercreutzia* 404257 and *Acetilactobacillus* (P<0.05) in CYR were higher than in mice in CCR (P<0.05) and CMR (P<0.05), respectively (Fig. 8b). Functional analysis of KEGG revealed that Cr (VI) inhibited the microbiota function of membrane transduction, translation, replication and repair, and lipid metabolism, while promoting the function of metabolism of terpenoids and polyketides, cofactors and vitamins. However, mice treated with CVP showed the reverse function of those pathways (Fig. 9a). MetaCyc analysis showed that Cr (VI) inhibited the microbiota function of Nucleoside and Nucleoside biosynthesis, and fatty acid and lipid biosynthesis, while promoting the function of amino acid biosynthesis in mice. However, CVP could restore the microbiota function of treated animals (Fig. 9b). The abundance of KEGG pathways of Aminoacyl-tRNA biosynthesis (P<0.05), bacterial secretion system (P<0.01), D-Alanine metabolism (P<0.05) were significantly higher in CCR, Phenylalanine metabolism (P<0.05), RNA polymerase (P<0.05) and beta-Lactam resistance (P<0.01) were significantly higher in CMR, while RNA degradation was signally higher in CYR (P<0.05) (Fig. 9c). The abundance of MetaCyc pathways of COA-PWY (P<0.05), Heme-Biosynthesis-II (P<0.05), Peptidoglycansyn-PWY (P<0.05), and Redcitcyc (P<0.05) were significantly higher in CCR, Centferm-PWY (P<0.05), Cobalsyn-PWY (P<0.05), P163-PWY (P<0.05), Salvadehypox-PWY (P<0.05) and Sulfate-CYS-PWY (P<0.05) were higher in CMR, while Argornprost-PWY (P<0.05), Glycolysis-E-D (P<0.05), PWY-7187 (P<0.05), PWY-7221 (P<0.05) and SO4ASSIM-PWY (P<0.05) were signally higher in CYR (Fig. 9d).

CVP-regulated intestinal microbiota metabolites of Cr (VI) induced mice: A total of 3391 (positive 2163, negative 1395) metabolites were identified in mice, with 35, 189, and 180 different metabolites between CCR and CMR, CMR and CRY, and CCR and CYR, respectively (Fig. 10a). The representative different metabolites between CCR and CMR were Dixyrazine (P<0.001), Erionyl Yellow AR (P<0.01), 2-Aminoisobutyric acid (P<0.01), 2-Aminobutyric acid (P<0.01), Dimethylglycine (P<0.01), and 4-Aminobutyric acid (GABA) (P<0.01). The typical different metabolites between CMR and CYR were Glucoiberin (P<0.0001), M413T284 (P<0.0001), Cellopentaose (P<0.0001), Erionyl Yellow AR (P<0.001), and 3-beta-Glucosylcellotriose (P<0.0001). The main different metabolites between CCR and CYR were N-acetylgalactosamine (P<0.0001), N-Acetylglucosamine (P<0.0001), 2-Benzylmalic acid (P<0.0001), and N-Acetylmannosamine (P<0.001). Further analysis found that Cr (VI) significantly increased the abundance of Cephamycin C (P<0.01), Erionyl Yellow AR (P<0.01), and decreased the abundance of N-(4-Methoxyphenyl)-2-(1-piperazinyl) acetamide in mice. However, animals treated with CVP emerged higher abundance of N-(4-Methoxyphenyl)-2-(1-piperazinyl) acetamide, and lower abundance of Cephamycin C (P<0.01) and Erionyl Yellow AR (P<0.01) (Fig. 10b). KEGG pathways of metabolites between CCR and CMR found that Taste transduction (P<0.05), Estrogen signaling pathway (P<0.05), GnRH

secretion (P<0.05), and Quorum sensing (P<0.05) were varying between the two groups. Pathways of Starch and sucrose metabolism (P<0.01), biosynthesis of nucleotide sugars (P<0.01), Phosphotransferase system (PTS) (P<0.01), O-Antigen nucleotide sugar biosynthesis (P<0.01), and Glucagon signaling pathway (P<0.05) were significantly different between CMR and CYR. Pathways of Starch and sucrose metabolism (P<0.0001), ABC transporters (P<0.01), Galactose metabolism (P<0.01), and Biosynthesis of nucleotide sugars (P<0.05) were markedly different between CCR and CYR (Fig. 11).

Spearman correlation analysis of physiological index and microbiota in mice induced by Cr (VI): Spearman correlation analysis found that microbiota from genera of *Allobaculum*, *Merdisoma*, *Angelakisella,* and *Lawsonibacter* were negatively associated with net weight rate, heart index, kidney index, T-AOC, GSH-Px, SOD, IL-10 and gene expression of Nrf-2 and IL-10, while the population of these bacteria were positively related to liver index, spleen index, AST, ALT, Bun, creatinine, MDA, Interleukin (IL-6, IL-1β), TNF-α, the gene expressions of IL-6, TNF-α and Bax (Fig. 12a-b).

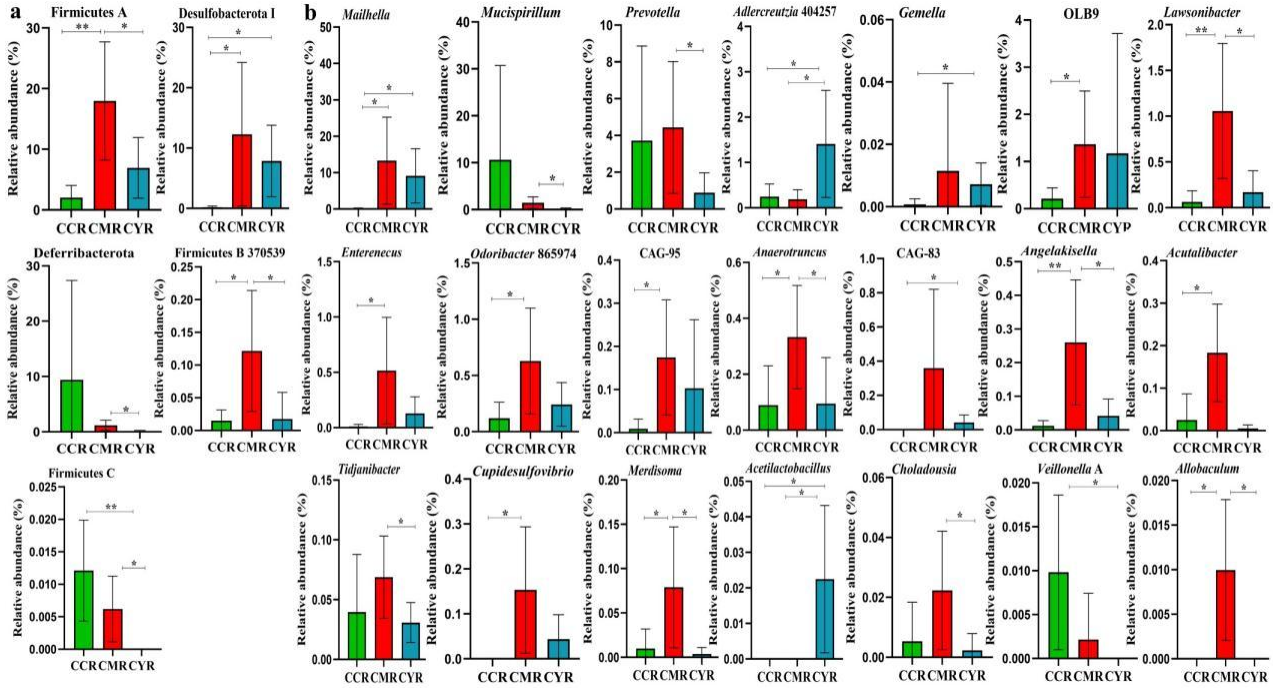

Fig. 8: Marker species of mice in various groups analyzed by ANOVA and t-test. a: phylum, b: Genus.

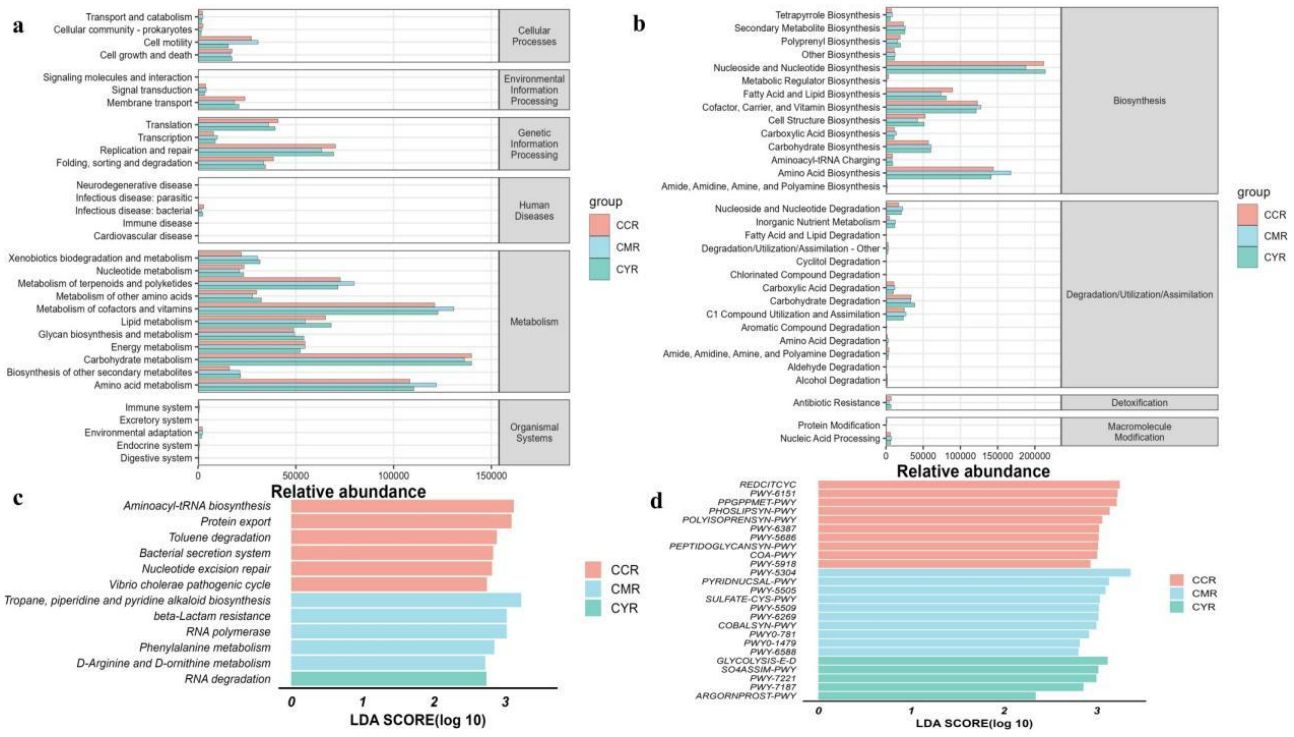

Fig. 9: Functional comparison of intestinal microbiota in different mouse groups. a: KEGG, b: MetaCyc.

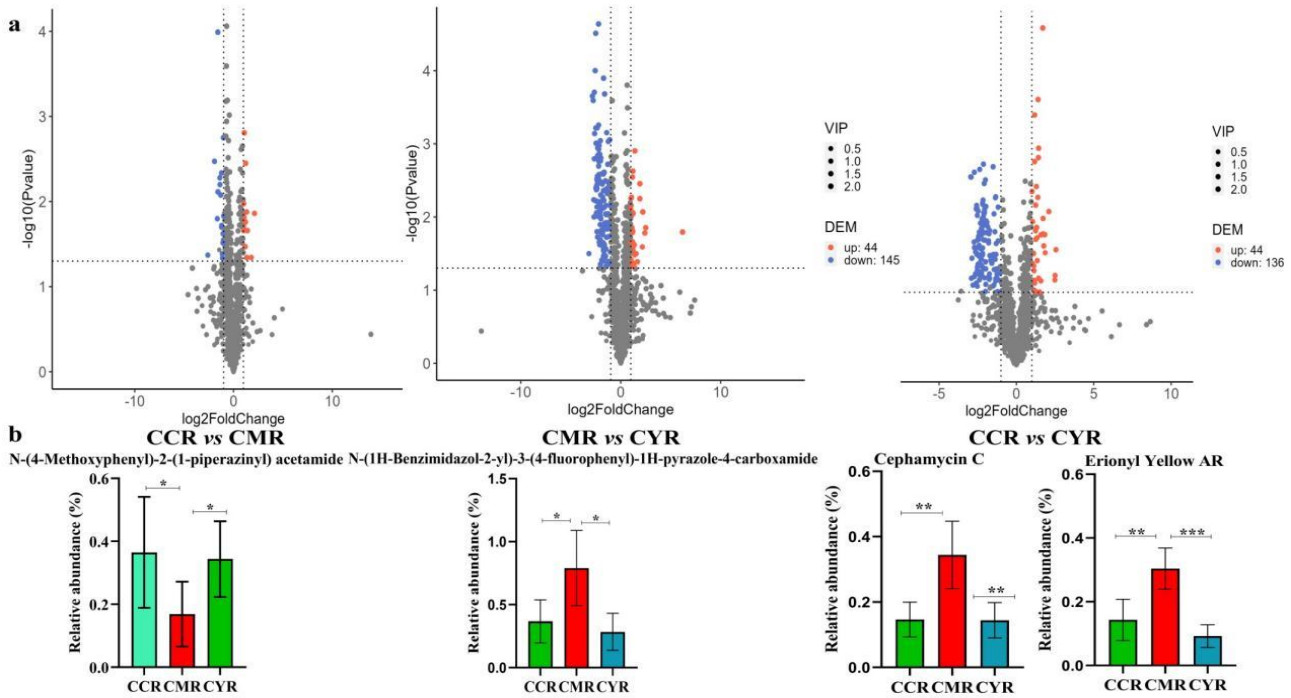

Fig. 10: Comparing the metabolites analysis in various mice groups. a: Volcano plot, Marker metabolites.

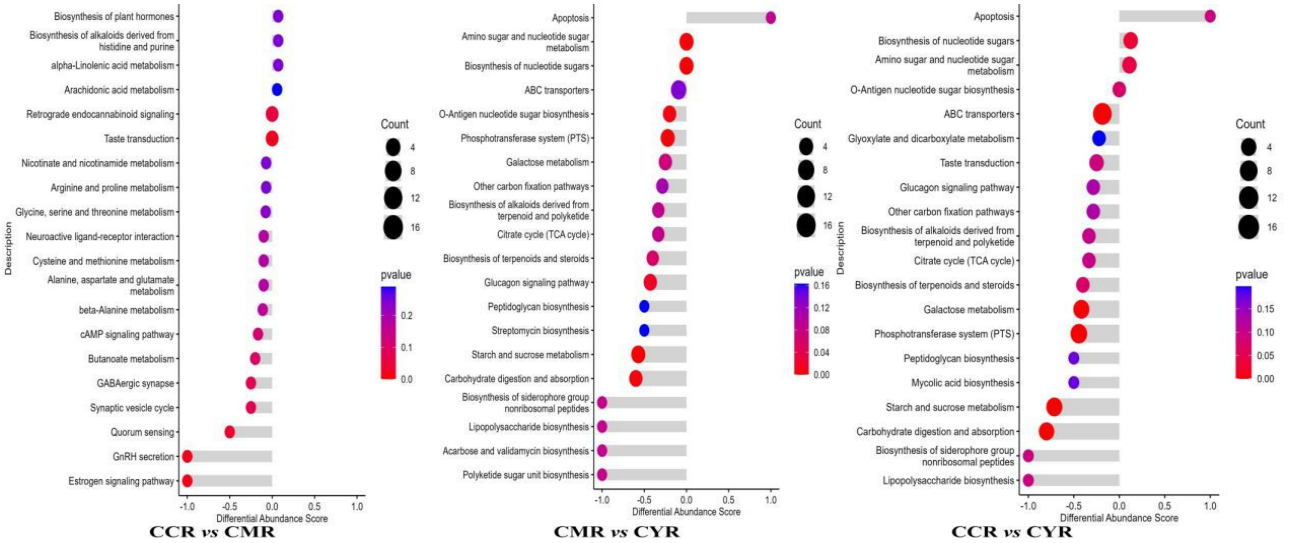

Fig. 11: Comparison of the analysis of KEGG pathways of metabolites in various groups of mice.

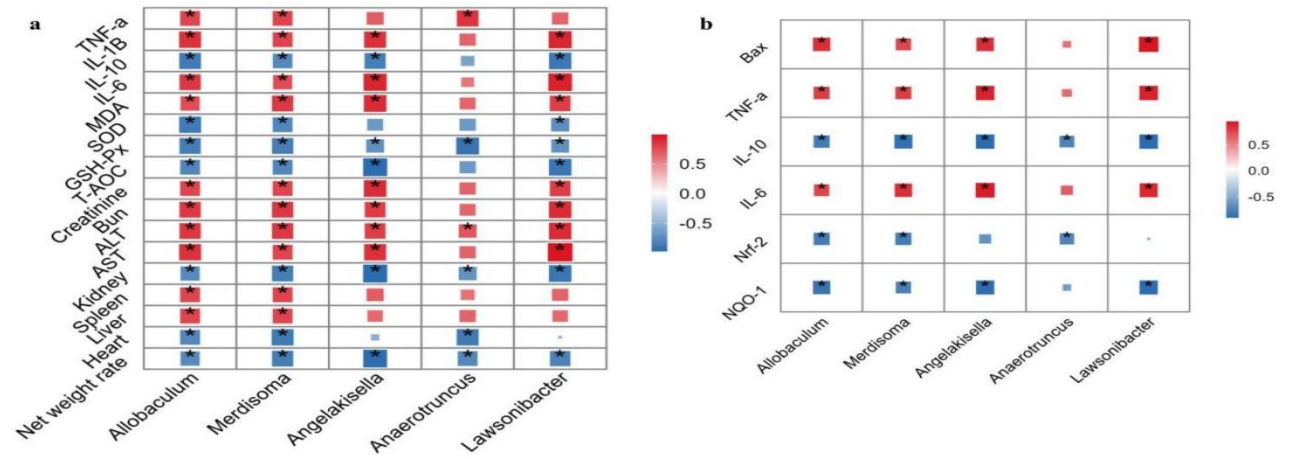

Fig. 12: Spearman correlation analysis of physiological indices, gene expressions, and microbiota in mice induced by Cr (VI). a: physiological indices, b: gene expressions.

DISCUSSION

The environmental contaminant Cr (VI) is a biologically poisonous and carcinogenic metal, which causes oxidative stress, genetic mutation, and apoptosis in mammals (Guo *et al.,* 2021). Here, we searched for the alleviation effect of CVP on liver and kidney injuries in mice induced by Cr (VI). Like previous studies, Cr (VI) negatively affects the body weight of mice (Islam *et al*., 2024) (Fig. 1). Moreover, Cr (VI) induced decreased heart and kidney indexes, while increasing the liver and spleen indexes in mice, as the results of that study were constant and like the finding of pervious research outcomes (Nauroze *et al*., 2023; Wang *et al*., 2023). Notably, CVP promoted animal growth by restoring organ indices in animals.

Histopathology analysis indicated that Cr (VI) caused liver and kidney damage with severe fibrosis in Liver/Kidney (Fig. 2), which was further confirmed by high levels of Aspartate Aminotransferase (AST), Alanine Aminotransferase (ALT), BUN, and Creatinine (Chen *et al*., 2019; Chen *et al*., 2022). CVP effectively relieved organ damage by regulating these indicators. Then we further examined oxidative resistance in mice; SOD, T-AOC, MDA, and GSH-Px are commonly used enzymes to indicate antioxidant ability (Xie *et al*., 2022). Oxidative damage was also reported in previous studies in animals induced by Cr, with higher MDA and lower T-AOC, GSH-Px, and SOD (Nauroze *et al*., 2023; Li *et al*., 2024; Zhou *et al*., 2025). The elevated levels of SOD, T-AOC, and GSH-Px demonstrated in Fig. 3a, and the lower level of MDA in treated animals indicated that CVP could enhance the antioxidant ability of mice. An important factor that keeps the balance of redox in cells is nuclear factor erythroid 2-related factor 2 (Nrf2), and it could regulate the generation of antioxidant proteins to protect cells from oxidative damage (Liu *et al*., 2024). There are two main important antioxidant response proteins include quinone oxidoreductase 1 (NQO-1) and Heme oxygenase 1 (HO-1) (Cao *et al*., 2021), and previous research indicated that increased Nrf2 as well as HO-1 are involved in the reduction of oxidative damage to the cell and inflammation (Li *et al*., 2023; Liu *et al*., 2024). In the present research, mice induced with Cr (VI) had lower gene expression levels towards Nrf2 factor ($P<0.001$), NQO-1 ($P<0.001$) and HO-1 ($P<0.01$), while mice treated with CVP had increased gene expression levels towards Nrf2 factor ($P<0.001$), NQO-1 ($P<0.01$) and HO-1 ($P<0.05$), which demonstrates that CVP remitted mice damages via regulating antioxidant capacity of mice. Then we examined inflammatory factors in mice and found that Cr (VI) lower the interleukin (IL) -10 ($P<0.05$) but higher level of IL-6 ($P< 0.01$), IL-1β ($P<0.001$) and Tumer Necrosis Factor-α (TNF-α) ($P<0.01$) which indicated the violent inflammatory response in mice, while CVP could reduce inflammation by regulating those factors. IL-6, IL-1β, and TNF-α were the major inflammatory cytokines, while IL-10 may be the anti-inflammatory factor (Tylutka *et al*., 2024). Other potential external factors include dietary composition, antibiotics and other medications, environmental pollutants, pathogens, stress, and host genetic background, all of which can alter gut microbial diversity and function. Relative gene expression also confirmed that CVP could upregulate IL-10 and prevent IL-6, IL-1β, and TNF-α expression (Fig. 3b). These results reveal that CVP mitigated organ damage by promoting oxidation resistance and suppressing inflammatory reactions. The two known key apoptosis regulators in cell apoptosis are Bax and Bcl-2 (Cosentino *et al*., 2022; Fu *et al*., 2022), while Bax is a pro-apoptotic protein that induces cell to apoptosis in cells (Fu *et al*., 2022). We also observed the gene and protein expression of Bax and found that Cr (VI) significantly up-regulated Bax ($P<0.001$), while CVP could inhibit it. Our results showed that CVP reduced the induced apoptotic activity by suppressing the expression of Bax.

Then we performed microbial sequencing and achieved 1296118 raw and 1198907 filtered sequences, which generated 33164 ASVs (Fig. 4a). Cr (VI) caused intestinal dysbiosis in different taxa (Fig. 5) and decreased Firmicutes / Bacteroidota (0.68) in CMR compared with CCR (1.17). F/B value is a frequently used dysbiosis indicator (Magne *et al*., 2020), and CVP significantly increased the ratio in the CYR group (1.06). Those results showed that CVP could restore the microbiota composition of mice, which was also reflected by the restored intestine function of animals (Fig. 9). The abundance of *Lactobacillus* at the genus level in CMR (7.72%), is lower than CCR (19.65%) and CYR (25.54%) (Fig. 5e). *Lactobacillus* is a probiotic genus that can restrict the colonization of pathogens, improve intestinal barrier integrity, reduce inflammation, and regulate immunity (Cicenia *et al*., 2014). The elevated abundance of *Lactobacillus* in treated animals further indicated that CVP could lower gut inflammation levels in mice.

There were five phyla and twenty-one genera that were different among the three mouse groups (Fig. 8), and among them, an increase in the population of *Lawsonibacter* was reported in obese people (Prykhodko *et al*., 2024) and in metabolic disorders (Huang *et al*., 2024). A higher abundance of *Anaerotruncu*s was determined in liver cancer-affected mice found (Zhang *et al*., 2021) and positively associated with irritable bowel syndrome (Wu *et al*., 2024), in mice with liver injury (Wu *et al*., 2023). Enriched *Angelakisella* was previously examined in obese mice (Plaza-Díaz *et al*., 2022) and follicular cyst sheep (Feng *et al*., 2021). An enriched *Allobaculum* was detected in rats with cardiotoxicity (Lin *et al*., 2021) and ulcerative colitis mice (Yang *et al*., 2024). Higher abundance of *Lawsonibacter* ($P<0.01$), *Anaerotruncu*s ($P<0.05$), *Angelakisella* ($P<0.01$) and *Allobaculum* ($P<0.05$) in Cr (VI) induced mice (Fig. 8), our results and previous studies showed that those genera were potential disease indicators, which was also confirmed by Spearman correlation analysis (Fig. 13). Treated mice had a lower abundance of that genus, that showed CVP relieved damage by regulating microbiota.

The association between serological and immuno-histochemical results and intestinal microbiota data in mice reflects a complex interplay between immune response and gut microbial composition. Serological markers, such as cytokine levels or specific antibodies, often indicate systemic inflammation or immune activation, while immunohistochemical analysis reveals localized tissue responses, including immune cell infiltration or expression of pro-inflammatory mediators in intestinal tissues (Peña-

Durán *et al*., 2025). These immune parameters are closely linked to shifts in the gut microbiota, whereas an imbalance in the population of pathogenic and beneficial microbes can exacerbate immune responses. Conversely, specific microbial taxa have been associated with protective effects, modulating immune responses and maintaining mucosal homeostasis. Therefore, alterations in microbiota composition correlate with both systemic and local immune changes, suggesting that the microbial population plays an essential role in experimental mouse models (Yoo *et al*., 2020). Metabonomic analysis found that 3391 metabolites were identified in mice (Fig. 10a), 4 vital indicators include N(1H-Benzimidazol-2-yl)-3-(4-fluorophenyl)-1Hpyrazole-4- carboxamide, Cephamycin C, Erionyl Yellow AR and N-(4-Methoxyphenyl)-2-(1-piperazinyl) acetamide in Cr (VI) induced mice (Fig. 10b). However, CVP could effectively decrease those metabolites. Microbial–metabolite interactions may collectively mitigate chromium-induced physiological impairments by restoring intestinal microbial balance and beneficial metabolite production. These metabolites can enhance antioxidant defenses, suppress inflammatory responses, and regulate apoptosis, thereby protecting hepatic and renal tissues from oxidative and cellular damage.

The limitations of the study integrate transcriptomic, metabolomic, and microbiota analyses, it does not explore causal mechanisms in depth, for instance, through knockout models or targeted inhibition of specific signaling pathways like Nrf2 or inflammatory cytokines. Additionally, the polysaccharide composition and purity were not validated using high-resolution structural techniques such as NMR or GC-MS, which limits reproducibility. Finally, the study was conducted in a controlled laboratory setting, and its translational relevance to humans or other animal models is yet to be tested.

Conclusion: In summary, we demonstrated that Tibetan *Coriolus versicolor* polysaccharide could effectively alleviate liver and kidney damage in mice exposed to chromium by regulating antioxidant ability, inflammatory response, apoptosis, and intestinal microbiota in mice. Our findings may contribute to developing novel therapeutics for heavy metal poisoning.

Data availability: All the generated data sequences were inserted into the NCBI database under accession number: PRJNA1238872.

Author contributions: KL, SL, ZY: Research idea and methodology; JW, SL, BS, ZS, KL: Laboratory reagents, materials, and analysis equipment; JW, KL: Writing the original draft and preparation; SL, MHA, ZY, KL: Review, writing, and editing; KL: Visualization and supervision; The final copy of the manuscript was approved by all contributing authors.

Conflict of interest: None.

Funding: This work was supported by the Base and Talent Project of the Science and Technology Program of Xizang, China (XZ202502JD0028).

Acknowledgement: The authors extend their appreciations to the Ongoing Research Funding Program (ORF-2026-191), King Saud University, Riyadh, Saudi Arabia

REFERENCES

Aljohani ASM, 2025. Chromium and nickel toxicity in sheep: pathophysiology and management approaches. Pakistan Veterinary Journal 45(1):62-72.

Alvarez CC, Bravo Gómez ME, Hernández Zavala A, 2021. Hexavalent chromium: Regulation and health effects. Journal of Trace Elements in Medicine and Biology 65:126729.

Balzerani F, Blasco T, Pérez-Burillo S, *et al*., 2024. q2-metnet: QIIME2 package to analyse 16S rRNA data via high-quality metabolic reconstructions of the human gut microbiota. Bioinformatics 40:btae455.

Bi S, Jing Y, Cui X, *et al*., 2024. A novel polysaccharide isolated from Coriolus versicolor polarizes M2 macrophages into an M1 phenotype and reverses its immunosuppressive effect on tumor microenvironment. International Journal of Biological Macromolecules 259:129352.

Cao J, Lu M, Yan W, *et al*., 2021. Dehydroepiandrosterone alleviates intestinal inflammatory damage via GPR30-mediated Nrf2 activation and NLRP3 inflammasome inhibition in colitis mice. Free Radical Biology and Medicine 172:386-402.

Che Q, Luo T, Shi J, *et al*., 2022. Mechanisms by which traditional Chinese medicines influence the intestinal flora and intestinal barrier. Frontiers in Cellular and Infection Microbiology 12:863779.

Chen L and Wang J, 2022. Gut microbiota and inflammatory bowel disease. WIREs Mechanisms of Disease 14:e1540.

Chen S, Xu C, Huang Y, *et al*., 2026. Polysaccharide of Xizang Coriolus versicolor mitigates spleen damage in mice exposed to chromium by regulating gut microbiota. Pakistan Veterinary Journal 46: 419-428.

Chen W, Wang W, Zhou L, *et al*., 2022. Elevated AST/ALT ratio is associated with all-cause mortality and cancer incidents. Journal of Clinical Laboratory Analysis 36:e24356.

Chen X, Wei W, Li Y, *et al*., 2019. Hesperetin relieves cisplatin-induced acute kidney injury by mitigating oxidative stress, inflammation and apoptosis. Chemico-Biological Interactions 308:269-278.

Chen X, Wu J, Fu X, *et al*., 2023. Fructus mori polysaccharide alleviates diabetic symptoms by regulating intestinal microbiota and intestinal barrier against TLR4/NF-κB pathway. International Journal of Biological Macromolecules 249:126038.

Cicenia A, Scirocco A, Carabotti M, *et al*., 2014. Postbiotic activities of lactobacilli-derived factors. Journal of Clinical Gastroenterology 48 Suppl 1, Proceedings from the 7th probiotics, prebiotics & new foods meeting held in Rome on September 8-10, 2013:S18-S22.

Cooper B and Yang R, 2024. An assessment of acquire X and compound discoverer software 3.3 for non-targeted metabolomics. Scientific Reports 14:4841.

Cosentino K, Hertlein V, Jenner A, *et al*., 2022. The interplay between BAX and BAK tunes apoptotic pore growth to control mitochondrial-DNA-mediated inflammation. Molecular Cell 82:933-949.

Douglas GM, Maffei VJ, Zaneveld JR, *et al*., 2020. PICRUSt2 for prediction of metagenome functions. Nature Biotechnology 38:685-688.

Fang S, Wang T, Li Y, *et al*., 2022. *Gardenia jasminoides* Ellis polysaccharide ameliorates cholestatic liver injury by alleviating gut microbiota dysbiosis and inhibiting the TLR4/NF-κB signaling pathway. International Journal of Biological Macromolecules 205:23-36.

Feng T, Ding H, Wang J, *et al*., 2021. Alterations of serum metabolites and fecal microbiota involved in ewe follicular cyst. Frontiers in Microbiology 12:675480.

Fu Y, Yuan H, Xu Y, *et al*., 2022. Protective effects of *Ligularia fischeri* root extracts against ulcerative colitis in mice through activation of Bcl-2/Bax signaling. Phytomedicine 99:154006.

Gariboldi MB, Marras E, Ferrario N, *et al*., 2023. Anti-cancer potential of edible/medicinal mushrooms in breast cancer. International Journal of Molecular Sciences 24:10120.

Goraya MU, Shahid R, Ashraf A, *et al.,* 2025. Selenium mitigates Paraquat-Induced hematotoxicity, oxidative stress, biochemical alterations, and nephrotoxicity in male Albino rats. Pakistan Veterinary Journal 45(3):1361-1368.

Guo S, Wang X, Wang L, *et al*., 2021. Inflammatory injury and mitophagy of the brain in chicken exposed to Cr(VI). Environmental Science and Pollution Research 28:42353-42361.

Habtemariam S, 2020. Trametes versicolor (Synn. Coriolus versicolor) polysaccharides in cancer therapy: targets and efficacy. Biomedicines 8:135.

He X and Li P, 2020. Surface water pollution in the middle Chinese Loess Plateau with special focus on hexavalent Chromium (Cr6+): occurrence, sources and health risks. Exposure and Health 12:385-401.

Hedberg YS, 2020. Chromium and leather: a review on the chemistry of relevance for allergic contact dermatitis to chromium. Journal of Leather Science and Engineering 2020:002.

Hsu CL and Schnabl B, 2023. The gut liver axis and gut microbiota in health and liver disease. Nature Reviews Microbiology 21:719-733.

Huang F, Deng Y, Zhou M, *et al*., 2024. Fecal microbiota transplantation from patients with polycystic ovary syndrome induces metabolic disorders and ovarian dysfunction in germ-free mice. BMC Microbiology 24:364.

Islam S, Sarkar O, Mukherjee S, *et al*., 2024. Chronic low-dose chromium VI exposure induces oxidative stress and apoptosis with altered expressions of DNA repair genes and promoter hypermethylation in the liver of Swiss albino mice. Journal of Applied Toxicology 44:1014-1027.

Katoh K and Standley DM, 2013. MAFFT multiple sequence alignment software version 7: improvements in performance and usability. Molecular Biology and Evolution 30:772-780.

Kazakis N, Kantiranis N, Kalaitzidou K, *et al*., 2017. Origin of hexavalent chromium in groundwater: The example of Sarigkiol Basin, Northern Greece. Science of the Total Environment 593-594:552-566.

Kim J, Kim K, and Kim W, 2021. Gut microbiota restoration through fecal microbiota transplantation: a new atopic dermatitis therapy. Experimental & Molecular Medicine 53:907-916.

Li C, Liu M, Deng L, *et al*., 2023. Oxyberberine ameliorates TNBS-induced colitis in rats through suppressing inflammation and oxidative stress via Keap1/Nrf2/NF-κB signaling pathways. Phytomedicine 116:154899.

Li N, Li X, Zhang X, *et al*., 2024. Low-dose hexavalent chromium induces mitophagy in rat liver via the AMPK-related PINK1/Parkin signaling pathway. PeerJ 12:e17837.

Li Y, Huang Y, Li Z, *et al*., 2022. Mechanisms of chromium isotope fractionation and the applications in the environment. Ecotoxicology and Environmental Safety 242:113948.

Liang X, Chen J, Xu C, *et al.,* 2025. Tupistra chinensis polysaccharide mitigates the inflammatory response by regulating gut-microbiota in mice induced by LPS. Pakistan Veterinary Journal 45(3):1353-1360.

Lin H, Meng L, Sun Z, *et al*., 2021. Yellow wine polyphenolic compound protects against doxorubicin-induced cardiotoxicity by modulating the composition and metabolic function of the gut microbiota. Circulation: Heart Failure 14:e008220.

Liu J, Zou B, Xiang C, *et al*., 2024. Comprehensive bioinformatics analysis unveils THEMIS2 as a carcinogenic indicator related to immune infiltration and prognosis of thyroid cancer. Scientific Reports 14:8156.

Liu M, Guan G, Wang Y, *et al*., 2024. p-Hydroxy benzaldehyde, a phenolic compound from Nostoc commune, ameliorates DSS-induced colitis against oxidative stress via the Nrf2/HO-1/NQO-1/NF-κB/AP-1 pathway. Phytomedicine 133:155941.

Magne F, Gotteland M, Gauthier L, *et al*., 2020. The firmicutes/bacteroidetes ratio: A relevant marker of gut dysbiosis in obese patients? Nutrients 12:1474.

Nauroze T, Ali S, Kanwal L, *et al*., 2023. Ameliorative effect of *Nigella sativa* conjugated silver nanoparticles against chromium-induced hepatotoxicity and renal toxicity in mice. Saudi Journal of Biological Sciences 30:103571.

Peña-Durán E, García-Galindo JJ, López-Murillo LD, *et al*., 2025. Microbiota and inflammatory markers: a review of their interplay, clinical implications, and metabolic disorders. International Journal of Molecular Sciences 26:1773.

Peng S, Xu C, He Q, *et al*., 2024. Fucoidan alleviates intestine damage in mice induced by LPS via regulation of microbiota. Pakistan Veterinary Journal 44:517-525.

Plaza-Díaz J, Manzano M, Ruiz-Ojeda FJ, *et al*., 2022. Intake of slow-digesting carbohydrates is related to changes in the microbiome and its functional pathways in growing rats with obesity induced by diet. Frontiers in Nutrition 99:992682.

Price MN, Dehal PS, Arkin AP, 2010. FastTree 2--approximately maximum-likelihood trees for large alignments. PLOS ONE 5:e9490.

Prykhodko O, Burleigh S, Campanello M, *et al*., 2024. Long-term changes to the microbiome, blood lipid profiles and IL-6 in female and male Swedish patients in response to bariatric Roux-en-Y gastric bypass. Nutrients 16:498.

Pushkar B, Sevak P, Parab S, *et al*., 2021. Chromium pollution and its bioremediation mechanisms in bacteria: A review. Journal of Environmental Management 287:112279.

Rahman MM, Islam F, Or-Rashid MH, *et al*., 2022. The gut microbiota (microbiome) in cardiovascular disease and its therapeutic regulation. Frontiers in Cellular and Infection Microbiology 12:903570.

Rau U, Kuenz A, Wray V, *et al*., 2009. Production and structural analysis of the polysaccharide secreted by Trametes (Coriolus) versicolor ATCC 200801. Applied Microbiology and Biotechnology 81:827-837.

Saleem M, Ali S, Javaid A, *et al.,* 2025. Antitoxic Effects of fennel (*Foeniculum vulgare*) extract against chlorpyrifos induced toxicity in rabbits. Pakistan Journal of Veterinary and Animal Research 1(2): 59-62

Song L, Yang J, Kong W, *et al*., 2023. Cordyceps militaris polysaccharide alleviates ovalbumin-induced allergic asthma through the Nrf2/HO-1 and NF-κB signaling pathways and regulates the gut microbiota. International Journal of Biological Macromolecules 238:124333.

Tarrah A, Callegaro S, Pakroo S, *et al*., 2022. New insights into the raw milk microbiota diversity from animals with a different genetic predisposition for efficiency and resilience to mastitis. Scientific Reports 12:13498.

Tu Y, Zhou Z, Shu C, *et al*., 2022. The crosstalk between saliva bacteria and fungi in early childhood caries. Frontiers in Cellular and Infection Microbiology 12:845738.

Tumolo M, Ancona V, De Paola D, *et al*., 2020. Chromium pollution in european water, sources, health risk, and remediation strategies: An Overview. International Journal of Environmental Research and Public Health 17:5438.

Tylutka A, cf Ł, Zembron-Lacny A, 2024. Level of IL-6, TNF, and IL-1β and age-related diseases: a systematic review and meta-analysis. Frontiers in Immunology 15:1330386.

Wang J, Liu C, Zhao Y, *et al*., 2023. Selenium regulates Nrf2 signaling to prevent hepatotoxicity induced by hexavalent chromium in broilers. Poultry Science 102:102335.

Wang X, Yang Z, Xu X, *et al*., 2020. Odd-numbered agaro-oligosaccharides alleviate type 2 diabetes mellitus and related colonic microbiota dysbiosis in mice. Carbohydrate Polymers 240:116261.

Wang Z, Dong B, Feng Z, *et al*., 2015. A study on immunomodulatory mechanism of Polysaccharopeptide mediated by TLR4 signaling pathway. BMC Immunology 16:34.

Want EJ, Masson P, Michopoulos F, *et al*., 2013. Global metabolic profiling of animal and human tissues via UPLC-MS. Nature Protocols 8:17-32.

Wen B, Mei Z, Zeng C, *et al*., 2017. Metax: a flexible and comprehensive software for processing metabolomics data. BMC Bioinformatics 18:183.

Wu S, Wen F, Zhong X, *et al*., 2023. Astragaloside IV ameliorates acute alcohol-induced liver injury in micevia modulating gut microbiota and regulating NLRP3/caspase-1 signaling pathway. Annals of Medicine 55:2216942.

Wu Y, Li S, Lv L, *et al*., 2024. Protective effect of *Pediococcus pentosaceus* Li05 on diarrhea-predominant irritable bowel syndrome in rats. Food & Function 15:3692-3708.

Xie N, Fan F, Jiang S, *et al*., 2022. Rhodiola crenulate alleviates hypobaric hypoxia-induced brain injury via adjusting NF-κB/NLRP3-mediated inflammation. Phytomedicine 103:154240.

Xu C, He Q, Zhu Z, *et al*., 2025. Propolis improves intestinal barrier function against *Cryptosporidium parvum* via NLRP6 inflammasome. mBio16(11):e0231725.

Yang T, Qin N, Liu F, *et al*., 2024. Berberine regulates intestinal microbiome and metabolism homeostasis to treat ulcerative colitis. Life Sciences 338:122385.

Yin J, Wang L, Chen Y, *et al*., 2019. A comparison of accumulation and depuration effect of dissolved hexavalent chromium (Cr6+) in head and muscle of bighead carp (Aristichthys nobilis) and assessment of the potential health risk for consumers. Food Chemistry 286:388-394.

Ying M, Yu Q, Zheng B, *et al*., 2020. Cultured Cordyceps sinensis polysaccharides modulate intestinal mucosal immunity and gut microbiota in cyclophosphamide-treated mice. Carbohydrate Polymers 235:115957.

Yoo JY, Groer M, Dutra SVO, *et al*., 2020. *et al*. Gut microbiota and immune system interactions. Microorganisms 8:1587.

Zhang D, Zhao G, Sun W, *et al*., 2023. Bile metabolites as diagnostic biomarkers for perihilar cholangiocarcinoma. Scientific Reports 13:3177.

Zhang X, Coker OO, Chu ES, *et al*., 2021. Dietary cholesterol drives fatty liver-associated liver cancer by modulating gut microbiota and metabolites. Gut 70:761-774.

Zhao L, Zhao J, Bai Z, *et al*., 2022. Polysaccharide from dandelion enriched nutritional composition, antioxidant capacity, and inhibited bioaccumulation and inflammation in Channa asiatica under hexavalent chromium exposure. International Journal of Biological Macromolecules 201:557-568.

Zhong L, Yan P, Lam WC, *et al*., 2019. Coriolus versicolor and ganoderma lucidum related natural products as an adjunct therapy for cancers: A systematic review and meta-analysis of randomized controlled trials. Frontiers in Pharmacology 10:703.

Zhou X, Yang X, Liu X, *et al*., 2025. Hexavalent chromium (Cr6+) induces oxidative stress, inflammatory response, apoptosis and DNA damage in the liver of largemouth bass by inhibiting the Nrf2-Keap1 signal pathway. Fish Physiology and Biochemistry 51:53.